AL42 - Effect of SO_2 Concentration and Humidity on the Removal of SO_2 from Cell Effluent Gases Using Hydrated Lime

Karthikeyan Rajan[1], Duygu Kocaefe[2], Yasar Kocaefe[3], Jonathan Bernier[4], Yoann Robert[5] and Yves Dargis[6]

1. Postdoctoral fellow, Industrial Materials Research Chair (CHIMI)
2. Professor, Director of Graduate Studies in Engineering – Research option, Holder of the Industrial Materials Research Chair (CHIMI)
3. Professor, Director of Applied Sciences Department

University Research Centre on Aluminium (CURAL), Aluminium Research Centre (REGAL)
University of Quebec at Chicoutimi, Chicoutimi, Quebec, Canada

4. Principal adviser and R&D program manager, Environment and Climate Change
5. Environment research scientist, Aluminium Technology Solutions

Rio Tinto, Arvida Research and Development Centre (ARDC), 1955, Boulevard Mellon, C.P 1250, Jonquière, Quebec, G7S 4K8

6. Account Manager

Graymont, 25, rue De Lauzon, Bureau 206 Boucherville, QC, Canada J4B 1E7
Corresponding author: Duygu_Kocaefe@uqac.ca

Abstract

To reduce the release of pollutants to the atmosphere, including SO_2, the control of atmospheric emissions can be necessary to respect air quality standards. In this work, a semi-dry method was used for the removal of SO_2 from the effluent gases of the aluminum electrolysis cells. The experimental investigation presented in this research work is to examine the possibility of the removal of low-concentration SO_2 from the gas with hydrated lime ($Ca(OH)_2$). The reaction was carried out between the hydrated lime and the gas containing different concentrations of SO_2 under dry and humidified conditions. The results indicate that the humidity plays a key role in the enhancement of the reaction between lime and SO_2. Furthermore, the surface area and morphological analyses suggest that the reactants have a strong interaction on the lime surface, which subsequently decreases the lime surface area available for further reaction with SO_2. The X-ray photoelectron spectroscopy (XPS) provided information on the chemical interactions taking place between lime and SO_2 species along with their conversion to $CaSO_3$/$CaSO_4$ products. The experimental results permitted the evaluation of the product ($CaSO_3$/$CaSO_4$) formation and the SO_2 removal efficiency with hydrated lime from a gas containing a low concentration of SO_2.

Keywords: Effluent gas desulfurization, Sulfur dioxide, Hydrated lime, Calcium sulfate.

1. Introduction

Due to the sulfur content in petroleum coke used in the anode manufacturing, aluminum smelters emit SO_2 to the atmosphere [1]. Depending on the quantity released and the airshed capacity, SO_2 emissions could have detrimental effects on human health and environment. To control the emissions of SO_2, the effluent gases from a process are desulfurized. A number of methods are used by the industry [1]. The desulfurization processes can be separated into two categories depending on the sorbent can be reused in a loop or not: regenerable and non-regenerable. The regenerable processes release the SO_2 from the sorbent which can be reused to capture other SO_2. In the non-regenerable processes, the sorbent reacts irreversibly with SO_2 to produce a byproduct such as gypsum that can be valorized. Both regenerable and non-regenerable processes are further classified into three types: dry [2], wet [3], and semi-dry [4]. In the wet process, the effluent gas is bubbled through a liquid column, thus producing a liquid product such as Na_2SO_4(aq). In the dry process, the effluent gas is put in contact with a dry sorbent. In the semi-dry process, the

sorbent is injected in the form of a slurry; the water vaporizes creating a highly humid environment [4]. The products containing the captured SO_2 may be subjected to further processing for valorization.

Alternative calcium sulfate raw materials are being developed due to increased industrial gypsum use. Calcium sulfate hemihydrates (β - $CaSO_4 \cdot 0.5\ H_2O$), known as high-intensity gypsum, have become increasingly popular because of their exceptional thermal stability, chemical resistance, and mechanical strength. The use of calcium sulfate is significant in construction materials, molding works, alternate binders [5,6]. The beneficial nature of gypsum produced as a byproduct of desulfurization process truly depends on its final quality. The presence of supplementary hazardous elements such as arsenic, mercury, lead, selenium, etc. could pose a threat to its applications. Researchers tried various approaches, including chemical modification, to produce good quality calcium sulfate materials [6]. However, it involves high cost, skilled manual labor, and special laboratory requirements, which would be difficult for construction applications where large quantities are needed. Also, the transformation of calcium containing raw materials to high-intensity gypsum should address the environmental challenges of pollution, sustainability and minimize the hazardous output as well as consider the economic viability [7] . The efficiency of product formation also reported to be based on the SO_2 adsorption rate by calcium containing particles. Many parameters, such as pH, additives, organic acids, help improve the adsorption rate on the surface of the particles. Seo et al. [8] reported that certain acids provide both the adsorption of SO_2 and a higher efficiency of the desulfurization product[8] Similarly, additives such as Na_2CO_3 and MgO have enhanced the alkalinity[9][10]. Liu et al. [11] studied the role of CO_2 in effluent gases containing SO_2 at concentrations of greater than 1000 ppm using lime[11]. However, their aim was to enhance the CO_2 capture along with SO_2. Though several researchers have investigated the removal of higher concentrations of SO_2 from a gas for the industrial applications, the removal of lower SO_2 concentrations remains difficult to achieve.

Due to the low cost and high abundance, lime (CaO), $Ca(OH)_2$, and limestone $Ca(CO)_3$ are used as a common source material to adsorb SO_2 [1,12]. However, because of the low thermal stability of limestone, it needs additional grinding steps before using it as an efficient desulfurization source. Thus, lime is preferred as the most common and effective sorbent source in desulfurization. Dasari et.al. [13] and Ruhland et al. [14]have studied the kinetic and absorption behavior of SO_2 in $Ca(OH)_2$ solutions. The instantaneous reaction with a low resident time yields the product $CaSO_3$. Kikkawa et al. [3] have investigated the role of the granular limestone size via wet desulfurization process. An SO_2 removal efficiency of 90 % has been achieved because of the use of granular limestone, but needed a neutralization column to ensure the rubbing of the limestone particles in order to expose a fresh lime surface to gas.[3]

In the current work, the desulfurization of effluent gas via a semi-dry process using hydrated lime ($Ca(OH)_2$), which produces calcium sulfite/sulfate as products, were explored. The concentration of SO_2 in the effluent gas coming from the electrolysis cells is much lower compared to that of the other processes such as power generating stations. The lower concentration of SO_2 could significantly change the composition of the final $CaSO_3/CaSO_4$ product. The quantity of specific components of the product was estimated through chemical species analysis. Physiochemical characterizations of the desulfurization product were performed using BET surface area analysis, X-ray photoelectron spectroscopy, and SEM analysis.

2. Experimental

2.1 Materials and Methods

The hydrated lime $Ca(OH)_2$ used for the current work is provided by Graymont industries, Canada. The powdered raw material has an average particle size of ~10 μm. All the experiments were carried out using hydrated lime as received without further processing. SO_2 and air were mixed and the desired concentration of SO_2 was adjusted with the help of mass flow controllers.

The reactions were carried out using a fixed bed reactor system composed of a custom-made reactor bed, a humidity-controlled chamber, and a pulsed fluorescence SO_2 analyzer. A schematic diagram of the experimental system is shown in Figure 1. The reaction takes place between hydrated lime and a mixture of SO_2 and air, with and without water (humidity). The temperature was kept constant at 100 °C for all the experiments. To carry out the experiments under humidified conditions, the humidity was produced with the help of a custom-made humidity chamber, and the relative humidity was maintained constant around 12 %. The sample weight was 100 mg. The reaction period was about 5 h for all the experiments.

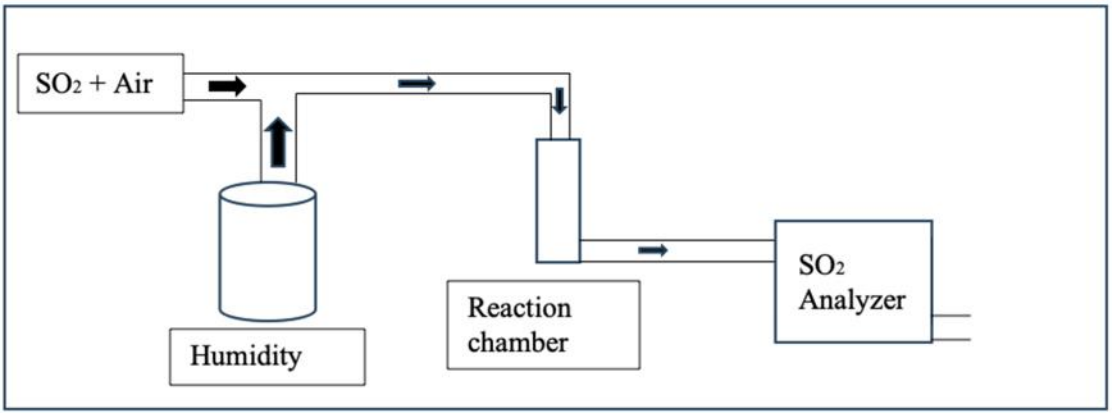

Figure 1. A schematic diagram of the semi-dry experimental set-up for effluent gas desulfurization.

2.2 Product Characterization

A variety of analytical methods were used to obtain the composition and properties of the hydrated lime and the products. The Micromeritics instrument (Gemini VII) was used to determine the surface area and the sorption properties through the BET surface area analysis. Degassing of the samples were prepared by Micromeritics FlowPrep 060 system. SO_2 concentration was recorded and analyzed with Thermo Scientific (iQ series 43) high level SO_2 analyzer. The morphology of lime was studied using a high-resolution scanning electron microscope (FEI Quanta FEG 200). The chemical properties of lime were investigated by an X-ray photoelectron spectroscopy using an ESCALAB 250 Xi (Thermo Fisher Scientific) with a monochromated Al K_α source at a power of 218.8 W (14.7 kV, 14.9 mA) and a 180˚ spherical sector analyzer at constant analyzer energy transmission mode. Standard charge compensation with low energy electrons and Ar+ ions was used. The pressure of the analysis chamber was around 10^{-6} Pa (10^{-8} mbar). Survey spectra were acquired at a pass energy of 150 eV and a step size of 1.0 eV. High resolution spectra were acquired at 20 eV pass energy and step size 0.1 eV. This yields a full width at half maximum (FWHM) for the ester peak in polyethylene terephthalate (PET) of 0.81 eV. Specimens were analyzed at an emission angle of 0˚ with respect to surface normal. Based on typical values for electron attenuation length, this yields an XPS analysis depth of 5-10 nm for a flat surface.

3. Results and Discussion

Table 1 shows the different cases with corresponding sample names and SO_2 concentrations in the effluent gas. The possible reactions involving lime and SO_2 in the presence of water vapor are shown below in Equations (1-6). The interaction between H_2O vapor and SO_2 gas could result in H_2SO_3 as illustrated in Equation (1) [1]. Further, the dissociation of H_2SO_3 could lead to the formation of SO_3^{2-} as shown in Equation (2). Similarly, SO_2 molecules could react with lime, which would produce $CaSO_3$ (equation (3)). Natural oxidation can occur in the effluent gas desulfurization reactions depending on the pH. As shown in Equation (4), oxygen in air can also react with SO_2, resulting in SO_3 formation; and this could further react with lime to produce $CaSO_4$ as given in Equation (5). As reported by Cordoba et al.[15], imposed conditions could help produce $CaSO_4 \cdot 2H_2O$. The typical scenario given in equation (3) is the common reaction to produce $CaSO_3$. The equation (6) shows that the calcium hydroxide could transform to calcium oxide by adding heat (indicated by Δ). Also, by adding heat, CaO could eventually react with SO_3 to form gypsum. Thus, there are two possible scenarios which could result in the formation of $CaSO_4$ (gypsum) as the final product.

Table 1. Experimental conditions.

Name of the sample	Relative humidity (RH, %)	SO_2 concentration (ppm)
SO_2 inlet – 80 ppm	12	80
SO_2 inlet – 120 ppm	12	120
SO_2 inlet – 160 ppm	12	160
SO_2 inlet – 160 ppm	0 (Dry)	160

$$SO_2(g) + H_2O\ (g) \rightarrow H_2SO_3\ (g) \quad (1)$$

$$H_2SO_3(g)\ \leftrightarrow 2H^+(g)\ + {SO_3}^{2-}\ (g) \quad (2)$$

$$Ca(OH)_2(s) + SO_2(g) \rightarrow Ca\,SO_3(s) + H_2O\ (g) \quad (3)$$

$$1/2O_2(g) + SO_2(g) \rightarrow SO_3(g) \quad (4)$$

$$Ca(OH)_2\ (s) + SO_3\ (g) \rightarrow Ca\,SO_4(s) + H_2O\ (g) \quad (5)$$

$$Ca(OH)_2\ (s) \xrightarrow{\Delta} CaO\ (s) + H_2O\ (g) \quad (6)$$

3.1 BET Analysis

The analyses of both the unreacted and reacted hydrated lime samples were carried out under the same conditions. The samples were degassed at 100 °C for 1 h to clean the surface contamination adsorbed from the environment. The analyses were carried out for a period of 24 h under liquid N_2. Isotherms of Figure 2 (a) show the BET surface area results of lime materials before and after reaction. The inset of the Figure 2 (a) shows the hysteresis behavior which belongs to the IUPAC type IV isotherms. This indicates that both lime samples contain micropores on their surfaces. The structural surface properties of the limes were determined using BET analysis. The results showed that the unreacted lime has a specific surface area of 27 m^2/g whereas the that of the reacted lime is 14 m^2/g. The relationship between pore width vs. pore volume was determined (Figure 2 (b)). The pore volumes of unreacted and reacted limes were found as 0.165 cm^3/g and 0.101 cm^3/g, respectively. The decrease in pore volume clearly indicates that the surface of the lime was in contact with the SO_2 containing gas, which consequently reacted to produce $CaSO_3/CaSO_4$.

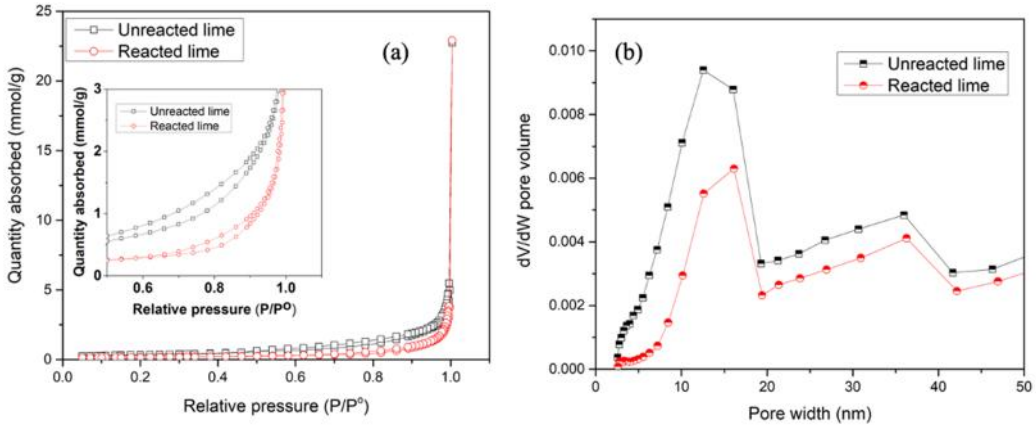

Figure 2. (a) BET results of unreacted and reacted lime (gas containing 160 ppm SO_2 at 12 % relative humidity) and (b) corresponding pore size distributions.

3.2 SEM Analysis

The morphological analyses were carried out for unreacted lime and lime reacted with gas containing 160 ppm SO_2 and 12 % relative humidity using SEM. The images are displayed in Figure 3. The surface morphology of the unreacted lime (Figure 3 (a)) appears to have sheets composed of lamellar microstructures. The individual grains of these microstructures have particles sizes less than 10 µm. On the other hand, the surface morphology of the reacted sample shown in Figure 3 (b) displays an agglomerated bulk structure in place of a lamellar microstructure. Also, the structure uniformity is less visible compared to that of the unreacted lime. As demonstrated by the BET results, SO_2 molecules have provoked significant changes in the surface topography of lime particles. The adsorbed SO_2 species, at the reaction temperature of 100 °C and in the presence of relative humidity of around 12 %, seem to transform a sheet-like microstructure of lime towards a granular structure, which results in the formation of non-uniform particles on the lime surface. Such structural changes did not occur when the reaction was carried out with dry gas (not shown).

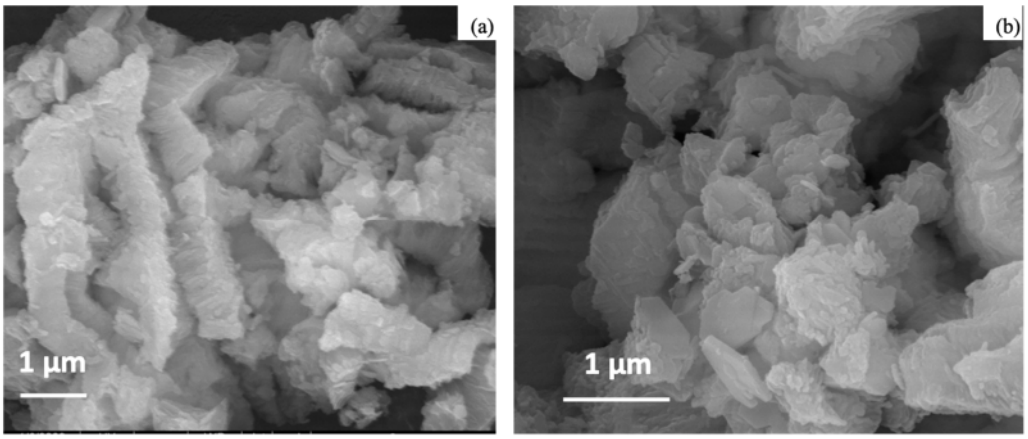

Figure. 3. SEM morphological analysis of (a) unreacted lime (b) lime reacted with gas containing 160 ppm SO_2 (RH ~12 %).

3.3 SO_2 Reaction Analysis

The reaction between SO_2 and lime with and without humidity were carried out, and the SO_2 outlet concentrations as a function of time are shown in Figure 4. The temperature of the reactions

was maintained at 100 °C and the inlet concentration of SO_2 was fixed at 160 ppm. The relative humidity was kept at 0 % for the dry experiment and at around 12 % during the experiment with humidified gas. The reaction could occur only if the SO_2 is adsorbed on the lime surface (external or in the pores). The more the reaction occurs in the bed, the lower the outlet concentration would be. As shown in this figure, in the absence of humidity, the SO_2 present in the inlet gas does not appear to react with lime (except at the very early stages), and the outlet concentration reaches rapidly the value at the inlet. This indicates that there is no interaction between SO_2 and lime, resulting in a stable curve of SO_2 concentration at 0.16 g/L (160 ppm) (the same as the mass concentration at the inlet). However, humidity significantly affects the reaction rate by improving the SO_2 adsorption, which is indicated by the SO_2 concentration that is lower than that of the inlet gas (around 0.14 g/L (140 ppm)). Clearly, the presence of humidity promotes the adsorption of SO_2 on the lime surface. The reaction continues even after 300 min since the outlet SO_2 concentration at this time is still less than the inlet SO_2 concentration.

Even though the humidity was kept constant as can be seen in Figure 5, periodic fluctuations of the SO_2 curve were observed in the case of experiments with humidity. These are due to the accumulation of water vapor after a certain period of time which led to droplet condensation in the line that absorbed SO_2. The experiments with humidity are quite tedious. Despite best efforts, the fluctuations could not be avoided and they were neglected in the analysis.

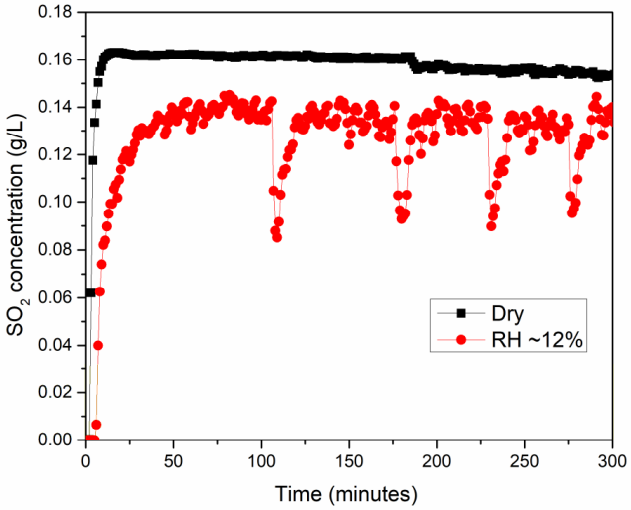

Figure 4. Evolution of outlet SO_2 concentration as a function of time under dry and humidified conditions (inlet SO_2 concentration: 160 ppm).

To understand the role of the inlet SO_2 concentration, the experiments were conducted at different SO_2 inlet concentrations (80 ppm, 120 ppm and 160 ppm) (Figure 5). All other experimental conditions were maintained constant at a RH of around 12 %. The outlet SO_2 concentrations are given as a function of time for the three cases.

In all three cases, initially (up to about 50 min), the reaction is fast which can be seen from the rapid increase in the outlet concentrations. Then, the rate slows down and remains more or less steady for the rest of the experiments. For the reaction to occur, SO_2 molecules have to go through first the external film outside the particle (external mass transfer resistance). The reaction can occur after the adsorption of SO_2 molecules onto the external particle surface. For the reaction within the interior of the particle, the SO_2 molecules have to diffuse into the pores (internal mass transfer resistance). Then, the adsorption of these molecules onto the solid surface in the pores would lead to the chemical reaction. It seems that the initial fast reaction rates correspond to the chemical reaction taking place on the external particle surfaces. Once the external surfaces of the

particles are reacted, the chemical reaction continues in the pores. But the presence of additional resistance slows down the reaction, resulting a steady rate observed as the reaction time increases.

When the reaction is complete, the outlet concentration should be the same as the inlet concentration. This was not reached in these experiments. For the 80 ppm experiment, the outlet SO_2 concentration was found to be around 0.040 to 0.045 g/L (40 to 45 ppm) (Figure 5(a)). For the 120 ppm and 160 ppm cases, the outlet concentrations are approximately 0.080 g/L (80 ppm) and 0.140 g/L (140 ppm), respectively (Figure 5 (b) and (c)). Thus, the reaction continues at a steady rate till the end (300 min). For the 80, 120, and 160 ppm cases, the outlet concentration reaches 56 %, 67 %, and 88 % of the corresponding inlet concentrations, respectively, at 300 min. This seems to indicate that the reaction rate increases with an increase in the inlet SO_2 concentration. Certainly, the presence of a greater number of SO_2 molecules provides a better opportunity for the reaction to proceed.

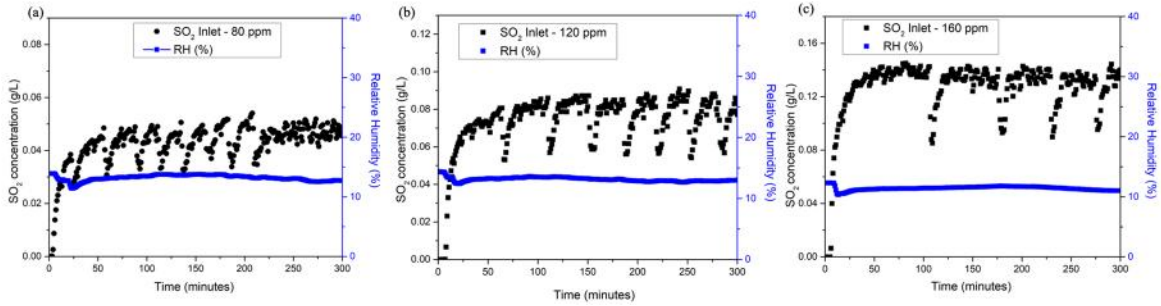

Figure 5. Outlet SO_2 concentration (g/L) vs. time (min) results for the reaction between lime and SO_2 at concentrations of (a) 80 ppm (b) 120 ppm (c) 160 ppm (RH ~12 %).

3.4 XPS Analysis

The XPS analyses were carried out to understand the surface reaction chemistry of unreacted and reacted samples. Their spectra are given in Figure 6. The reacted sample is hydrated lime material reacted with humidified gas containing 160 ppm SO_2 at 100 °C for 5 h. The calcium 2p spectra in Figure 6 (a) illustrates that the unreacted lime and the lime reacted with SO_2 have a significant peak shift observed at the $2p_{3/2}$ and $2p_{1/2}$ spin-orbit components. The difference in the shift from 346.5 eV to 347 eV for $2p_{3/2}$ and 350 eV to 351 eV for $2p_{1/2}$ could be the result of the attachment of heavy SO_2 molecules to the calcium species. The Figure 6 (b) complements these results with the presence of sulfur 2p spectra of the reacted sample. Similarly, the oxygen 1s spectra (Figure 6 (c)) clearly show that the shift in the peak position and peak intensity pointing out to the presence of reaction.

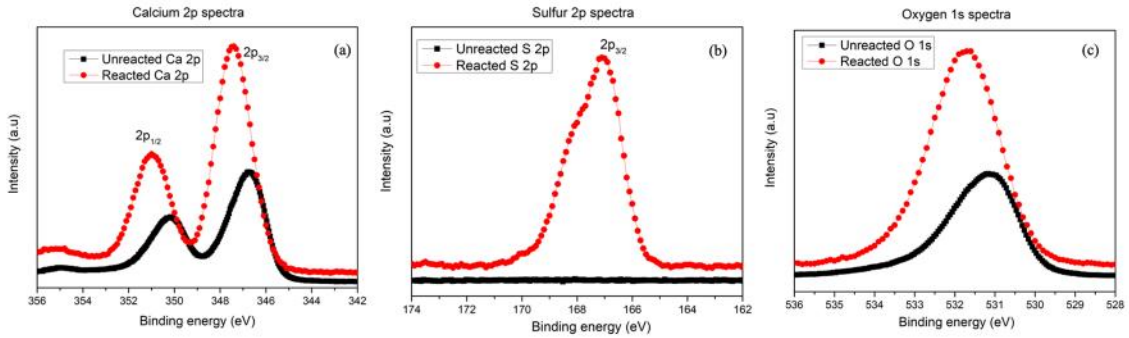

Figure 6. XPS analysis of (a) Calcium 2p, (b) Sulfur 2p, and (c) Oxygen 1s spectra for unreacted lime and lime reacted with 160 ppm SO_2 (RH ~12 %).

To understand the product formation and their chemical composition in detail, peak-fitting analyses were carried out on the samples reacted with gas containing different inlet SO_2 concentrations (Figures 7, 8, and 9). The parameters such as reaction temperature (100 °C), reaction period (5 h), relative humidity (~12 %), and lime quantity (100 mg) were maintained constant. The XPS analysis for the S 2p spectra of the desulfurization products is presented in Figure 7. Table 2 shows the corresponding data for respective chemical species and their peak area. The chemical species of the reacted samples were identified by fitting their spectra as shown in Figure 7. In all the S 2p spectra, there are two strong distinctive peaks at 166.9 eV and 168 eV. These peaks are related to the sulfur spectra of $2p_{3/2}$ and $2p_{1/2}$ spin-orbit components of SO_3^{2-}. The presence of SO_3^{2-} confirms the product formation of $CaSO_3$. Similarly, the chemical species of SO_4^{2-} $2p_{3/2}$ and $2p_{1/2}$ components are present at ~168.5 eV and ~169.6 eV. For both chemical species, the difference between the spin-orbit coupling for $2p_{3/2}$ and $2p_{1/2}$ is close to 1.1 eV and their intensity ratio is half of their original counterpart (~0.5)[16]. This is well matched with the formation of sulfur compounds, as reported by Chang et al[17]. Compared to the $CaSO_4$, formation of $CaSO_3$ compound is dominant when SO_2 concentration is low (80 ppm). When the inlet SO_2 concentration increased to 120 ppm (Figure 7 (b)), the percentage of $CaSO_4$ in the product increased to 10.5 %. Increasing the concentration of SO_2 further (160 ppm) did not significantly increase the $CaSO_4$ formation. The corresponding changes (decreasing) were observed for the formation of $CaSO_3$.

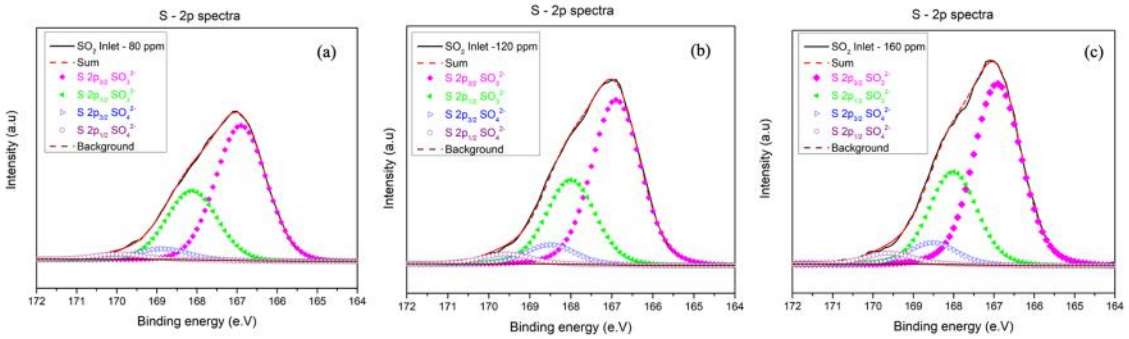

Figure 7. XPS analysis of S 2p spectra for experiments with inlet gas containing different SO_2 concentrations (a) 80 ppm (b) 120 ppm (c) 160 ppm.

Table 2. Summary of Sulfur 2p spectra.

Details	Peak area (%)	
Binding Energy (eV)	*166.9 and 168*	*168.5 and 169.6*
Chemical species	SO_3^{2-}	SO_4^{2-}
SO_2 inlet – 80 ppm	92.7	7.3
SO_2 inlet – 120 ppm	89.5	10.5
SO_2 inlet – 160 ppm	89.4	10.6

To understand further, the unresolved Ca 2p spectra were analyzed as shown in Figure 8. Table 3 gives a summary of the peak areas proportional to the product formation. The peak positions at ~347 eV and ~351 eV belong to the category of $2p_{3/2}$ and $2p_{1/2}$, respectively. The unresolved $2p_{3/2}$ spectra of calcium were fitted as given in the XPS binding energy manual [16,18] and their chemical species were identified. For all the different SO_2 concentrations, a small peak at 346.9 eV corresponding to CaO or $CaCO_3$ chemical structure is obtained. Though, the samples before and after reaction were handled with care and kept at an air-tight container, as mentioned by Liu et al. [11] the CO_2 present in the environment could influence the surface nature of calcium hydroxide at low temperature[11]. Further, two different chemical species were identified at 347 and 347.8 eV, which belong to $CaSO_3$ and $CaSO_4$, respectively. The peak shift was observed compared to the reported value of 348.3 eV for $CaSO_4$ which could be due to the overlapping of

multiple species at the same peak position. The peak position at 350.9 eV belongs to $CaSO_3$ chemical species with the spin-orbit counterpart of $2p_{1/2}$. Irrespective of the SO_2 concentrations, $CaSO_3$ peak is observed always at the same position. The overall peak area was calculated for the chemical species of $CaSO_4$ and $CaSO_3$ (Table 3). Once again, the dominant product formation is found to be $CaSO_3$ in all experiments. For the SO_2 inlet concentration of 80 ppm, it is observed that a higher amount of unreacted lime is present. This percentage decreased as the concentration of SO_2 (160 ppm) increased. This is in good agreement with the experimental data. For the same bed size, the 80 ppm inlet concentration resulted in the least product formation, and the 160 ppm inlet concentration gave the most product formation. SO_2 adsorbed on the solid lime surface was converted to the products of $CaSO_3$ and $CaSO_4$. Also, the amount of $CaSO_4$ increased with increasing inlet concentration of SO_2.

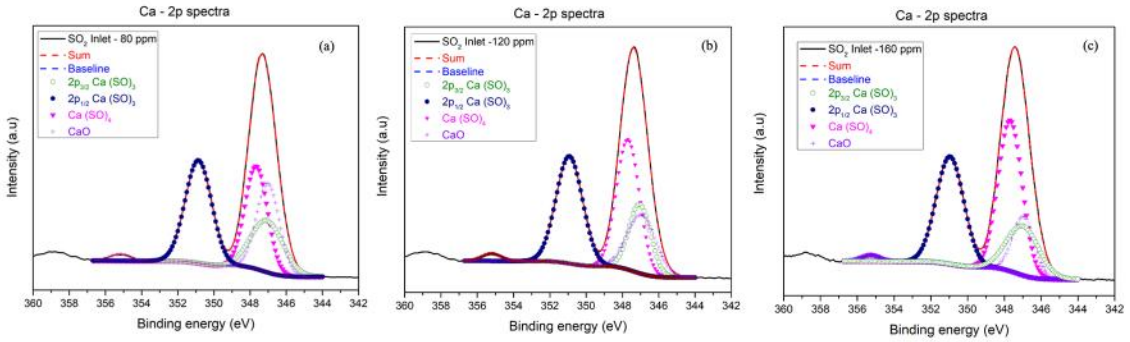

Figure 8. XPS analysis of Ca 2p spectra for experiments with gas containing different inlet SO_2 concentrations (a) 80 ppm (b) 120 ppm (c) 160 ppm.

Table 3. Summary of calcium 2p spectra.

Details	Peak area (%) Ca 2p		
Binding Energy (eV)	*~347.8*	*347 & 350.9*	*346.9*
Chemical species	$Ca(SO)_4$	$Ca(SO)_3$	CaO
SO_2 inlet – 80 ppm	26.4	50.2	23.4
SO_2 inlet – 120 ppm	33.1	48.0	18.9
SO_2 inlet – 160 ppm	38.5	47.9	13.6

To study the role of oxygen, O1s spectra were used to the investigate the formation of $CaSO_3$ and $CaSO_4$ compounds. The peaks were fitted as shown in Figure 9 and their corresponding peak areas are presented in Table 4. When the concentration of SO_2 was low, the oxygen species have contributed more to the formation of $CaSO_3$ than to the formation of $CaSO_4$ compounds. The unreacted surface oxygen O^- was found as 10.5 % at the lowest inlet SO_2 concentration. However, as the inlet concentration of SO_2 increased, the formation of $CaSO_3$ and $CaSO_4$ increased, and the amount of O^- decreased significantly. The trend is not uniform for different inlet SO_2 concentrations (120 and 160 ppm) compared to Ca 2p and S 2p spectra. This could be due to the presence of atmospheric oxygen from the XPS instrument. But the product of the experiment with 160 ppm of SO_2 has the highest amount of $CaSO_4$. This is similar to the results observed from Figure 7 (c), and it is in agreement with the results of the desulfurization experiments. The chemical composition analysis of the XPS results indicated that the dominant quantity produced was $CaSO_3$. According to our knowledge, the quantification and the detailed chemical species identification of the product formation for the SO_2 desulfurization reactions at low SO_2 concentrations has never been reported in the literature.

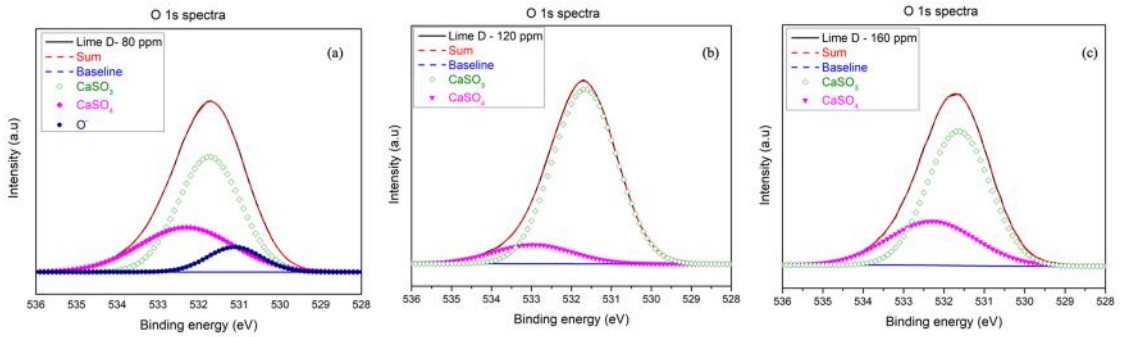

Figure 9. XPS analysis of O 1s spectra for experiments with gas containing different inlet SO_2 concentrations (a) 80 ppm (b) 120 ppm (c) 160 ppm.

Table 4. Summary of Oxygen 1s spectra.

Details	Peak area (%)		
Binding Energy (eV)	*532.3*	*531.6*	*529.2*
Sample details	$CaSO_4$	$CaSO_3$	O^-
SO_2 inlet – 80 ppm	32.8	56.7	10.5
SO_2 inlet – 120 ppm	11.9	87.8	0.3
SO_2 inlet – 160 ppm	31.4	68.4	0.2

4. Conclusions

The semi-dry gas desulfurization reactions were carried out with hydrated lime to study the desulfurization of effluent gas containing low SO_2 concentrations. The experiments were carried out to better understand the desulfurization process. The results could be helpful to develop technologies to eventually reduce SO_2 emissions coming from aluminum production. The hydrated lime with an average particle size of about 10 µm was used to carry out the reactions. It was found that the relative humidity plays a key role in the reaction of SO_2 with hydrated lime. The surface structural properties from BET analysis showed that the adsorbed SO_2 molecules modify the surface structure significantly. The experimental results indicated also that the higher the inlet SO_2 concentration is, the greater the amount of reacted lime particles is. The corresponding XPS results show that the product formed even at lower concentrations of SO_2 (such as 80 ppm). The chemical species at respective binding energy values indicated that the product contains a lower quantity of $CaSO_4$ and a greater quantity of $CaSO_3$. However, $CaSO_4$ formation increased with increasing inlet SO_2 concentration. According to the best of our knowledge, for low SO_2 concentrations (a few hundred ppm), this is the first study which identifies the different components of effluent gas desulfurization products through chemical composition analysis.

5. Acknowledgements

The financial and technical support of the NSERC, Rio Tinto, Graymont, CQRDA (MEI), University Research Centre on Aluminium (CURAL), the University of Quebec at Chicoutimi (UQAC) and Aluminium Research Center (REGAL) is greatly appreciated.

6. References

1. Nadeesha H. Koralegedara et.al, Recent advances in flue gas desulfurization gypsum processes and applications – A review, *J Environmental Management,* 2019*,* 251, 109572, 1–33.

2. L.J. Muzio and G.R. Often, Assessment of dry sorbent emission control technologies part I. fundamental processes, *J Air Pollution Control Association, 1987,* 37, 642–654.
3. Hirofumi Kikkawa et.al, New wet FGD process using granular limestone, *Ind Eng Chem Res,* 2002*,* 41, 3028–3036.
4. T. Zaremba et.al, Properties of the wastes produced in the semi-dry FGD installation, *J Thermal Anal Calorimetry,* 2008, 93, 439–443.
5. Guerra-Cossío M. A et.al, Calcium sulfate: An alternative for environmentally friendly construction, *EcoGRAFI- 2nd International Conference on Bio-based Building Materials & 1st Conference on ECOlogical valorisation of GRAnular and FIbrous materials, June 21st -June 23rd,* 2017, Clermont-Ferrand, France, AJCE - Special issue, 1–6.
6. Christian Pritzel et.al, Binding materials based on calcium sulphates *Cementitious Materials: Composition, Properties, Application,* 2017, Walter de Gruyter GmbH, 285–309.
7. Swift W M et.al, *Decomposition of calcium sulfate: A review of the literature,* Argonne national laboratory, U.S. energy research administration report, 1976, 1-64.
8. Sung Kwan Seo et.al, A study on the desulfurization efficiency of limestone sludge with various admixtures, *Journal of the Korean Ceramic Society*, 2015, 52, 479–482.
9. Jan B W Frandsen et.al, Optimisation of a wet FGD pilot plant using fine limestone and organic acids*, Chemical engineering science,* 2001, 56, 3275- 3287.
10. R. del Valle-Zermeño et.al, Synergistic effect of the parameters affecting wet flue gas desulfurization using magnesium oxides by-products, *Chemical Engineering Journal,* 2015, 262, 268–277.
11. Chiung-Fang Liu et.al, Effect of SO_2 on the reaction of calcium hydroxide with CO_2 at low temperatures, *Ind Eng Chem Res,* 2010, 49, 9052–9057.
12. Ravi K. Srivastava et.al, SO_2 Scrubbing Technologies: A Review, *Environmental progress,* 2001, 20, 219–228.
13. Dasari Ram Babu et.al, Absorption of sulfur dioxide in calcium hydroxide solutions, *Ind. Eng. Chem. Fundamental,* 1984*,* 23, 370–373.
14. Frank Ruhland et.al, The kinetics of the absorption of sulfur dioxide in calcium hydroxide suspensions, *Chemical Engineering Science,* 1991, 46, 939–947.
15. Patricia Córdoba, Status of Flue Gas Desulphurisation (FGD) systems from coal-fired power plants: Overview of the physic-chemical control processes of wet limestone FGDs, *Fuel,* 2015*,* 144, 274–286.
16. John F Moulder et.al, *Handbook of X-ray Photoelectron Spectroscopy A Reference Book of Standard Spectra for Identification and Interpretation of XPS Data, Book,* 1993, 1-260.
17. Chang Jing Yang et.al, Preparation of high-reactivity Ca-based SO_2 adsorbent and experimental study for simulated flue gas dry desulfurization, 2023 the 7th International Conference on Energy and Environmental Science (ICEES 2023), January 6–8, 2023, Changsha, China *Energy Reports,* 9**,** 85–95.
18. Christopher D Easton et.al, Practical guides for x-ray photoelectron spectroscopy: Analysis of polymers, *Journal of Vacuum Science & Technology A,* 2020, 38, 023207, 01-26.